Cement and Concrete Research 42 (2012) 656–664

Contents lists available at SciVerse ScienceDirect

Cement and Concrete Research

journal homepage: http://ees.elsevier.com/CEMCON/default.asp

Multicomponent gas diffusion in hardened cement paste at temperatures up to 350 °C

Gregor J.G. Gluth [a,*], Weiqi Zhang [b], Maria Gaggl [b], Bernd Hillemeier [a], Frank Behrendt [b]

[a] Institute for Civil Engineering, Technische Universität Berlin, Gustav-Meyer-Allee 25, 13355 Berlin, Germany
[b] Institute for Energy Engineering, Technische Universität Berlin, Fasanenstr. 89, 10623 Berlin, Germany

ARTICLE INFO

Article history:
Received 15 May 2011
Accepted 2 February 2012

Keywords:
Microstructure (B)
Mercury porosimetry (B)
Diffusion (C)
Cement paste (D)
Gas separation

ABSTRACT

Diffusional gas transport of a H_2/CO_2 mixture versus N_2 in the pore system of hardened cement pastes was studied at four temperatures up to 350 °C in a Wicke-Kallenbach cell. The pastes possessed separation factors α_{H_2,CO_2} from 1.42 to 3.43, i.e. the diffusion of hydrogen took place considerably faster than the diffusion of carbon dioxide. The separation factors depended on the threshold radii of the pastes, smaller threshold radii leading to higher separation factors. The Knudsen numbers of the controlling constrictions of the pore system and the temperature dependence of the effective diffusion coefficients of the gases show that gas transport in these constrictions takes place in the transient regime between Knudsen diffusion and bulk diffusion, smaller constriction widths leading to predominating Knudsen diffusion. It is therefore possible to use cement paste membranes to separate gas components of low molecular weight from higher weight components.

1. Introduction

Hardened cement paste (hcp) is a highly porous material with pore sizes ranging from fractions of nanometers to several hundreds of micrometers. The pore structure of the hcp influences, inter alia, its strength and modulus of elasticity as well as its durability by controlling the ingress of deleterious substances [1,2].

In principle, there are three possible gas diffusion mechanisms in porous solids [3]: bulk diffusion, Knudsen diffusion, and surface diffusion. Which mechanism prevails depends on many parameters such as pore size, surface chemistry of the pore walls, gas species, temperature, and pressure. When there is a gradient in total pressure, viscous flow can take place in addition to diffusion. The transport mechanism determines the rate of gas transport and its dependence on ambient conditions.

Although it is sometimes stated that different gas transport mechanisms can occur in hcp, most studies focus on measuring effective diffusivities and relating them to the mix-design of the investigated pastes or concretes. There are only a few studies concerned with the kind of mass transport that takes place inside the pores of hcp. Furthermore, these studies yield contradictory results: Schwiete and co-workers [4,5] concluded that gas transport in concrete specimens that were several decades old was governed by bulk diffusion and surface diffusion. In contrast, Därr and Ludwig [6] cited results according to which in "finely porous cement specimens" Knudsen diffusion prevails, while in hardened cement pastes gas transport takes place by bulk diffusion; surface diffusion occurred only when the diffusing gas was ethane. In a recent study Sercombe et al. [7] concluded that gas transport in hcp at atmospheric pressure takes place in the transient regime between bulk diffusion and Knudsen diffusion. Vu et al. [8] were able to model gaseous diffusion in hcp by assuming the Bosanquet equation is valid and assigning only pores with diameters of about 3–700 nm to the paste, by that implicitly assuming that Knudsen diffusion is an important mechanism for the gas transport in the paste. In addition, gas permeability measurements at varying mean pressures, interpreted by means of the Klinkenberg expression, provided evidence of Knudsen diffusion contributing considerably to gas flow in concretes, mortars and cement pastes [9–12].

In the present study a new application for hcp was investigated, which is related to its pore system and the gas transport mechanisms within. Due to economic and urgent ecological demands, new energy sources have to be found. One promising possibility is the production of fuel gas by wood gasification [13]. However, one problem associated with wood gasification is the comparatively low fuel value of the product gas. This arises because the product gas contains large amounts of carbon dioxide and nitrogen when air is used for partial oxidation [13,14]. It would therefore be beneficial to separate the hydrogen (high fuel value) in the product gas from the other components. Furthermore, by re-feeding the carbon dioxide-rich residual gas to the gasification reactor, the overall efficiency of the gasification process can be improved by shifting the chemical equilibria.

Except for high purity demands, gas separation by means of membranes is widely used and is regarded as the most cost-effective separation process [15,16]. In general, organic polymeric membranes are

* Corresponding author at: BAM Federal Institute for Materials Research and Testing, Unter den Eichen 87, 12205 Berlin, Germany. Tel.: +49 30 8104 3300; fax: +49 30 8104 1717.
E-mail addresses: gregor.gluth@bam.de (G.J.G. Gluth), frank.behrendt@tu-berlin.de (F. Behrendt).

0008-8846/$ – see front matter © 2012 Elsevier Ltd. All rights reserved.
doi:10.1016/j.cemconres.2012.02.001

employed for gas separation. However, polymeric membranes cannot be used at high temperatures or in aggressive chemical environments [17]. This also applies to the separation of the wood gasification products, since the product gas initially has a temperature of about 500–1000 °C and for operational reasons should not be cooled down too much before treatment. For the aforementioned reasons, inorganic membrane materials such as carbon and zeolites constitute a large area of research (see, e.g. Refs. [17–19]). However, these materials can have certain other drawbacks, such as brittleness, poor reproducibility, low fluxes, and fouling; in particular, they are much more expensive than polymeric membranes — more than 3000 US$/m^2 for some membrane modules [15,17,18,20].

The separation ability of porous inorganic membranes depends on the diffusion mechanisms within and, therefore, on their pore structure [15,21]. Since hcp contains pores in the nanometre range, it can be conjectured that Knudsen diffusion takes place inside its pore system, at least partly, and therefore hcp should also be able to separate gases. Thus, hcp may potentially be able to serve as cost-efficient inorganic membrane material for the processing of the wood gasification product. This was investigated in the present study by measuring separation factors and diffusivities of H_2, CO_2 and N_2 in hcp membranes. In addition, the insights gained into the diffusion mechanisms in hcp may ultimately lead to a proper modelling of the inflow of deleterious gases such as carbon dioxide into cementitious materials.

2. Background

2.1. Mean free path and Knudsen number

The mean free path is the average distance travelled by a molecule between two consecutive collisions with other molecules. For an ideal gas, the mean free path λ_i of the molecules is given by [22]:

$$\lambda_i = \frac{RT}{\sqrt{2}\pi d_i^2 p} \cdot \frac{1}{N_A}, \tag{1}$$

where R is the ideal gas constant, T is the absolute temperature (K), d_i is the diameter of the molecules, assumed to be rigid spheres (m), p is the pressure (Pa), and N_A is Avogadro's constant (mol^{-1}).

When a gas or a gas mixture diffuses in a porous medium or a single pore, the mean free path of the molecules might be greater or smaller than the pore size. The ratio of mean free path and pore size is called the Knudsen number, $Kn = \lambda/d_P$, where d_P is the pore diameter in the case of cylindrical pores.

2.2. Bulk diffusion

For small Knudsen numbers ($Kn << 1$) the molecules collide with each other much more frequently than with the pore walls. Diffusion in this regime is called molecular diffusion or bulk diffusion.

In this case, the fluxes of the n components of a gas mixture are related to the mole fractions and mole fraction gradients by the Maxwell–Stefan equation, which reads for ideal gases [3,23]

$$-\nabla x_i = \sum_{j=1; j\neq i}^{n} \frac{x_j J_i - x_i J_j}{c_t Đ_{ij}} \tag{2}$$

with the additional constraint

$$\sum_{i=1}^{n} \nabla x_i = 0 \tag{3}$$

for pure diffusion, i.e. no pressure gradient. In Eqs. (2) and (3), ∇x_i is the mole fraction gradient of component i (m^{-1}), x_i is its mole fraction, J_i is its molar flux (mol m^{-2} s^{-1}), c_t is the total molar concentration (mol m^{-3}), and $Đ_{ij}$ is the binary Maxwell–Stefan diffusion coefficient for the components i and j (m^2 s^{-1}).

For dilute gases, the diffusion coefficients $Đ_{ij}$ in Eq. (2) can be calculated from [23]

$$Đ_{ij} = \frac{3\sqrt{2}}{16\sqrt{\pi}} \cdot \frac{R^{1.5} T^{1.5}}{\sigma_{ij}^2 p \Omega_{ij}} \cdot \sqrt{\frac{1}{M_i} + \frac{1}{M_j}} \cdot \frac{1}{N_A}, \tag{4}$$

where σ_{ij} is the arithmetic mean of the Lennard–Jones collision diameters of the components i and j (m), Ω_{ij} is the collision integral for diffusion – a dimensionless function of the temperature and the Lennard–Jones characteristic energy ε_{ij} – and M_i and M_j are the molar masses of the components i and j (g/mol), respectively.

When neglecting the collision integral (i.e. putting $\Omega_{ij} = 1$), it follows from Eq. (4) that the $Đ_{ij}$ are temperature dependent by $T^{1.5}$. Since the collision integral is a function of the temperature too, the temperature dependence of the $Đ_{ij}$ is more accurately given as $T^{1.65\ldots2.0}$ [23].

2.3. Knudsen diffusion and transient regime

When the Knudsen number is large ($Kn >> 1$), there are virtually no molecule–molecule collisions but only molecule–wall collisions. This type of diffusion is called Knudsen diffusion and in this regime the different species of a gas mixture diffuse independently of each other. The flux of each species in a single cylindrical pore is then given by [23]

$$J_i = -c_t D_i^K \nabla x_i, \tag{5}$$

where

$$D_i^K = \frac{d_p}{3} \cdot \sqrt{\frac{8RT}{\pi M_i}}. \tag{6}$$

D_i^K is called the Knudsen diffusion coefficient. From Eq. (6) it can be seen that gases of low molecular weight will exhibit higher fluxes than gases of higher molecular weight under otherwise identical conditions.

For $Kn \approx 1$, when there are molecule–molecule as well as molecule–wall collisions, the correct expression for the fluxes remains controversial in the literature (see, e.g. Ref. [24]). However, one has to expect that with increasing Kn the Knudsen diffusion regime will increasingly prevail and Eq. (5) in connection with Eq. (6) is more suitable for describing the fluxes. Since the mean free path of common gases can be calculated to be in the range of 50–200 nm at atmospheric pressure and moderate temperatures, Knudsen diffusion is expected to occur to an appreciable extent in pores of diameters smaller than about 200 nm under these conditions.

2.4. Diffusion in porous solids

When dealing with diffusion in a porous solid, the fluxes are normally given per cross sectional area of the solid. Additionally, instead of the actual mole fraction gradients, the mole fraction differences between the two sides of the solid are considered, i.e. the porous solid (membrane) is treated as continuous medium:

$$J_i^{eff} \equiv \frac{N_i}{A_M t} = -c_t D_i^{eff} \cdot \frac{\Delta x_i}{L}, \tag{7}$$

where N_i is the amount of substance i (mol) flowing through cross sectional area of the membrane A_M (m^2) per time t (s), D_i^{eff} is the effective diffusion coefficient (m^2 s^{-1}), Δx_i is the difference of the mole fractions of substance i between the two sides of the membrane, and L is the thickness of the membrane (m).

In a porous solid only part of the cross sectional area is available for gas transport (described by accessible porosity and/or constriction factor) and the mole fraction gradients are lessened because of longer diffusion paths (described by tortuosity). Therefore, the fluxes per unit cross-sectional area of the porous medium are by a factor smaller than in free media or a single tube [25].

Surface diffusion can also contribute to mass transport in porous media. However, appreciable surface diffusion is restricted to solids of high surface area, i.e. solids with a large volume of small pores (d_P<10 nm) [15] such as microporous zeolites and carbons. The diffusion in micropores is quite different from bulk diffusion and Knudsen diffusion, and is considered elsewhere (e.g. Refs. [3,26]).

3. Experimental

3.1. Materials

Membranes for the diffusion measurements were made from two different Portland cements, one microfine binder based on blast furnace slag and Portland cement clinker, and one slag cement. For the slag cement pastes, fly ash was used as addition. Silica fume was used as addition for one of the Portland cement pastes. The chemical compositions of the binders are shown in Table 1 together with their abbreviated names, used throughout this paper. Seven pastes were prepared with different water/binder ratios (w/b) as shown in Table 2. In the low w/b pastes (w/b = 0.30 or smaller) PCE superplasticizer was used as supplementary.

Mixing of the pastes was done for 6 min in a mixer according to DIN EN 196–1. The pastes were cast in cubes of edge length of 100 mm. The cubes were covered and stored in the laboratory at 20 °C and 65% RH. After 24 h the pastes were demoulded and transferred into a water bath at approximately 20 °C. After an additional 6 days, cores (51 mm in diameter) were drilled from the hardened pastes and membranes of a thickness $L = 5$ mm were cut from the cores and polished. No slices from the top or the bottom of the cubes were used because of possible segregation. All membranes were cleaned in an ultra sonic water bath to remove residual dust from cutting and polishing. The membranes were subsequently transferred back into the water bath. The samples for the pore structure analyses were produced parallel to the membranes.

After a total hydration time of 28 days, all specimens were removed from the water bath and were oven-dried at 105 °C until constant weight was obtained, defined as the state where mass loss was less than 0.1% within 24 h.

Table 1
Compositions of binders.

Compound[a]	Amount in weight %					
	Portland cement 1 (PC1)	Portland cement 2 (PC2)[b]	Microfine binder (MF)	Slag cement (SC)	Fly ash (FA)	Silica fume (SF)
CaO	62.04	67.69	46.40	47.43[c]	4.69	<0.40
SiO_2	20.15	24.57	32.39	31.61[c]	51.41	98.43
Al_2O_3	4.49	2.05	8.52	10.37[c]	25.62	0.21
Fe_2O_3	2.29	0.33	0.53	0.84[c]	6.69	<0.20
MgO	2.41	0.58	6.12	6.15[c]	1.92	<0.20
MnO	0.03	<0.03	–	n.d.	0.08	<0.03
Na_2O	0.27	<0.20	0.29	n.d.	0.83	<0.20
K_2O	1.03	<0.10	0.44	n.d.	3.95	0.37
TiO_2	0.22	0.08	1.10	n.d.	1.05	<0.03
P_2O_5	0.21	0.33	<0.05	n.d.	0.50	<0.05
SO_3	2.81	1.91	1.54	0.71	0.99	0.73
LOI	3.21	0.97	0.18	1.01	2.18	0.74

[a] SO_3 determined by wet chemical analysis according to DIN EN 196–2; LOI according to DIN EN 196–2; all other values by XRF.
[b] White Portland cement.
[c] Manufacturer's data (XRF).

Table 2
Mix proportions of pastes.

Compound	Amount in g dm^{-3}						
	PC1 (0.25)	PC2 (0.25)	PC2 (0.45)	PC2 + SF (0.25)	MF (0.30)	SC + FA (0.20)	SC + FA (0.37)
Cement	PC1: 1762.2	PC2: 1762.2	PC2: 1303.0	PC2: 1344.8	MF: 1556.5	SC: 1245.1	SC: 962.3
Addition	–	–	–	SF: 336.2	–	FA: 560.3	FA: 433.1
Water	440.6	440.6	586.3	420.3	467.0	367.3	511.0
w/b	0.25	0.25	0.45	0.25	0.30	0.20	0.37

During all steps of later handling of the membranes, viz. transport and installation in the diffusion cell as well as after the diffusion measurements, the membranes showed neither cracks nor other signs of disintegration, i.e. they were mechanically stable.

3.2. Diffusion measurements

Diffusion measurements were performed in a steady-state setup according to the Wicke-Kallenbach method [26]. Fig. 1 shows a schematic of the employed diffusion cell. In this setup the gases flow laterally across the two surfaces of the membrane in slits of 2.5 mm width, the gases on either side of the membrane moving in opposite directions (counter-current flow). The membranes were tightened in the diffusion cell using flexible graphite seals. The diffusion cell can be heated; the temperature of the membrane was measured by a thermocouple.

The feed side of the membrane (left side in Fig. 1) was fed with a mixture of 49.8% H_2 and 50.2% CO_2 by volume. The permeate side (right side in Fig. 1) was swept with N_2 to maintain mole fraction gradients of H_2 and CO_2. The gases were fed to the membrane with flow rates of 30 cm^3 min^{-1}. All gases used were dry, high purity gases. H_2 and N_2 are assumed to be inert with respect to the hcp; the reaction of CO_2 with hcp is inhibited under dry conditions [27]. The total pressures on the two sides of the membrane were kept at $p = (1.050 \pm 0.005) \cdot 10^5$ Pa.

Before each measurement, the diffusion cell with the membrane was heated to 350 °C and kept at this temperature for 90 min. Then, the gases were allowed to flow for 30 min to purge the equipment and the membrane of residual substances and to reach steady-state diffusion. The outflowing gas mixtures on each side of the membrane were then analysed using a gas chromatograph. Subsequently, the temperature of the setup was lowered to 200 °C, 100 °C and room temperature (32 ± 5 °C) in successive steps, each step taking 15–30 min. The composition of the outflowing gases was recorded again after each step.

From the gas compositions, the separation factor α_{H_2,CO_2} of the membranes was calculated as usual [28] from

$$\alpha_{H_2,CO_2} = \frac{x_{H_2}'' / x_{CO_2}''}{x_{H_2}' / x_{CO_2}'}, \tag{8}$$

where x_{H_2}'' and x_{CO_2}'' are the mole fractions of H_2 and CO_2 in the permeate gas (at the outlet), respectively and x_{H_2}' and x_{CO_2}' are the mole fractions of H_2 and CO_2 in the feed gas, respectively.

Because of the high time spent on each experiment and the high number of mix-designs that were tested, only one membrane per mix-design was measured. Also, the dimensions of membranes were smaller than recommended for testing the gas permeability of concretes [29,30]. However, the much better homogeneity of cement paste as compared to concrete and mortar (absence of aggregates), great care in mixing, casting and selecting the specimens as well as the internal consistency of the results obtained, led us to believe

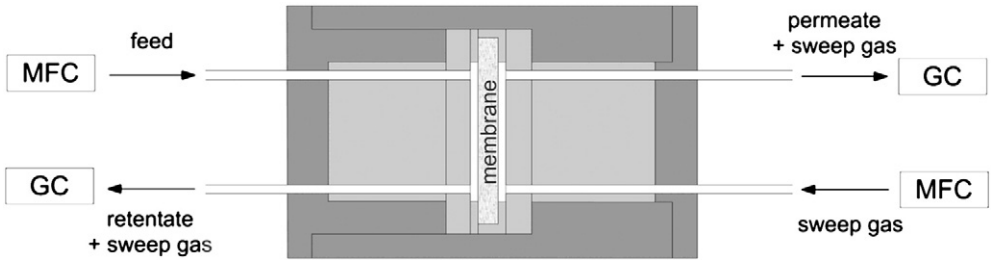

Fig. 1. Schematic of the employed diffusion cell. GC: gas chromatograph, MFC: mass flow controller.

that the membranes tested were representative of the respective materials.

3.3. Heat treatment

Samples for pore structure analyses were subjected to heat treatment in order to approximately emulate the decomposition processes at the beginning of the diffusion measurements. Since the samples were considerably larger than the membranes, the treatment in an electric oven was chosen as follows: heating to 350 °C within 30 min; maintaining the temperature for 24 h; cooling down to 105 °C within 24 h; cooling down to room temperature in a desiccator over silica gel.

3.4. Pore structure analysis

Mercury porosimetry measurements were performed on single samples with a volume of approx. 6 cm^3. Conversion from intrusion data to pore radii r_P was carried out by means of the Washburn-Laplace equation, $\Delta p = 2\gamma\cos\theta/r_P$, assuming cylindrical pores. The surface tension was taken as $\gamma = 0.480$ N/m, the contact angle θ was assumed to be 141.3°. The highest attainable mercury pressure was $2 \cdot 10^8$ Pa.

From the mercury porosimetry results the threshold radius r_{thr} [31,32] of the pastes was determined. This is commonly done by drawing tangents on the steep and the flat part of the cumulative distribution curve and taking the radius at their intersection as the threshold radius. However, Härdtl [33] found that the pore radius at which the slope of the cumulative distribution curve exceeds 0.1 $cm^3\,g^{-1}\,\mu m^{-1}$ is nearly identical to the threshold radius determined by graphical means. This kind of analysis is independent of the evaluation of where to draw the tangents. Therefore, in this study, the threshold radii were generally determined by the procedure proposed by Härdtl. In one case (PC2 + SF after heat treatment), the slope of the cumulative distribution curve was comparatively steep even for large pore radii; thus, in this case the threshold radius was determined using the graphic procedure.

Nitrogen adsorption isotherms were determined by the manometric method at liquid nitrogen temperature. The measurements were performed on ground samples with particle sizes in the range of 800–2000 µm. Before measurement, the samples were oven-dried again for 24 h and then degassed for 2 h at room temperature at a pressure of 7 Pa.

The micropore volume (d_P<~2 nm) was calculated by means of the *t*-plot method [34,35]. The *t*-curve of Lippens et al. [36] was used for the analysis. The linear part of the *t*-plots extended over $t \approx 0.3$–0.7 nm for all specimens and the *t*-plot was extrapolated from this range. The specific surface area a_S of the specimens was determined by the BET method [37,38]. The BET-plot was fitted over the relative pressure range $p/p^0 = 0.05$–0.25; the molecular area of nitrogen in the monolayer was assumed to be $a_m = 0.162$ nm^2, as usual.

The open porosity ε of the pastes was calculated from their apparent and bulk densities. Helium pycnometry was performed on the same grit as for nitrogen adsorption to measure the apparent density. The bulk density was calculated from oven-dried weight and bulk volume, determined by weighing specimens under water and in the saturated surface-dry state.

From the open porosities and the surface areas of the pastes, the hydraulic radius r_h of their open pore system was calculated from

$$r_h = \frac{V_P}{a_S} = \frac{\varepsilon}{a_V}, \tag{9}$$

where V_P is the open pore volume ($m^3\,g^{-1}$), a_S is the specific surface area ($m^2\,g^{-1}$), ε is the open porosity (%) and a_V is the surface area per unit volume of adsorbent ($m^2\,m^{-3}$).

4. Results

4.1. Pore structure of non-heat treated pastes

The mercury porosimetry curves of the investigated specimens before heat treatment are shown in Fig. 2; the threshold radii are given in Table 3 together with the open porosities. As documented in numerous earlier studies, lowering w/b led to smaller threshold radii and reduced open porosities. The use of slag containing cements (MF, SC) or pozzolanic materials (FA, SF) caused a further decrease of r_{thr} and ε. This effect – a more discontinuous and finer pore structure as a result of the use of slag or pozzolans – is also well-known and has been reported in many papers, some of which were summarised by Taylor [2].

The nitrogen adsorption isotherms of all pastes were of Type II with H3-hysteresis loops. Such hysteresis loops are typical of solids containing mainly slit-shaped pores [38]. The isotherm of MF(0.30) possessed a wide hysteresis loop while the shapes of the isotherms of the other pastes were similar to that of SC + FA(0.20), as shown in Fig. 3(A).

The desorption curve of MF(0.30) exhibited a marked, steep drop-off at $p/p^0 \approx 0.50$ (Fig. 3(B)). This is indicative of a high fraction of its pore volume being located behind pore entries with radii of $r_P = 2.5$ nm or smaller [39–41]. This again explains the noticeably

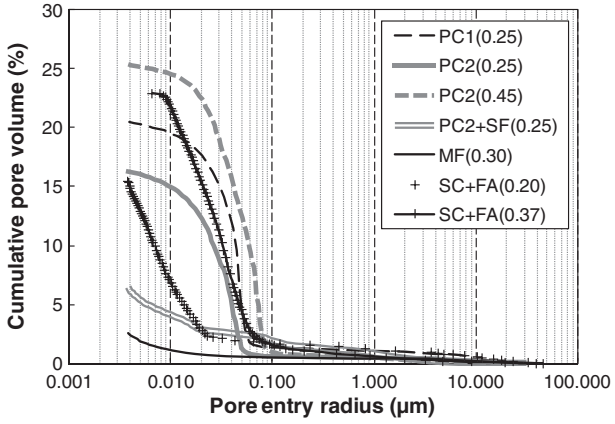

Fig. 2. Mercury porosimetry results of the non-heat treated cement pastes.

Table 3
Results of pore structure analyses of non-heat treated and heat treated pastes.

Paste	r_{thr} (nm)		ε (%)		a_S ($m^2\ g^{-1}$)		a_V ($m^2\ cm^{-3}$)		r_h (nm)	
	–	350 °C	–	350 °C	–	350 °C	–	350 °C	–	350 °C
PC1 (0.25)	62	78	21.7	22.4	4.89	6.74	9.19	12.69	23.6	17.7
PC2 (0.25)	56	61	16.1	18.5	4.60	5.27	9.03	10.11	17.8	18.3
PC2 (0.45)	92	96	25.0	26.0	7.49	7.82	11.93	12.30	20.9	21.1
PC2 + SF (0.25)	22	20	7.3	10.4	1.23	2.68	2.22	4.72	32.9	22.1
MF (0.30)	20	28	7.5	13.2	4.50	10.18	7.73	17.12	9.7	7.7
SC + FA (0.20)	29	38	8.5	13.6	3.49	5.83	6.45	10.58	13.2	12.9
SC + FA (0.37)	82	103	19.1	22.9	8.87	10.15	13.34	15.35	14.3	14.9

–: non-heat treated; 350 °C: heat treated.

small slope of the mercury porosimetry curve of paste MF(0.30) and its small mercury porosity (Fig. 2): in the measurements the smallest accessible pore radius was ~3.7 nm (corresponding to the maximum mercury pressure of $2 \cdot 10^8$ Pa), so that a lot of pore space remained unfilled.

The specific surface areas, together with the hydraulic radii calculated from these values and the open porosities, are shown in Table 3. The measured specific surface areas ranged from 1.23 to 8.87 $m^2\ g^{-1}$. Similarly low surface areas for pastes with low w/b – down to 0.50 $m^2\ g^{-1}$ for hcp with w/b = 0.20 – have been reported in other studies [42,43]. The comparatively low surface areas of the pastes studied here are partly due to the collapse of small pores during the harsh oven-drying procedure [44,45] and, probably, partly due to the partial carbonation of the hcp during drying and storage [46]. The hydraulic radii of the pastes showed no clear trend regarding the influence of the mix proportions or the kind of binders used.

Consistent with the small BET specific surface areas, all analysed pastes possessed micropore volumes smaller than 0.0005 $cm^3\ g^{-1}$, which is assumed to fall within the range of accuracy of the measurements. The absence of mensurable microporosity is also due to the collapse of small pores during oven-drying [45].

4.2. Effect of heat treatment on pore structure

Table 3 shows that heat treatment of the hcp specimens led to higher open porosities. The increase in ε was particularly marked for the pastes containing slag or pozzolanic materials. Since the decomposition of calcium hydroxide normally take place at temperatures higher than 350 °C [2], it can be assumed that the increase of open pore volume after temperature treatment is due to the decomposition of the other main components of hcp (C-S-H, AFm, AFt) and the opening of initially closed pores.

The mercury porosimetry curves of the heat treated pastes are shown in Fig. 4; it can be seen that their general character changed only slightly compared to the pastes without heat treatment. Although in some cases the mercury porosities increased considerably, only small changes in the threshold radii resulted from the heat treatment (Table 3). This is in line with the findings of Farage et al. [11], who also observed no systematic change in the threshold radius of hcp due to temperatures up to 300 °C.

The heat treatment caused only slight changes in the shape of the nitrogen adsorption isotherms of the pastes, though it led to a moderate widening of the hysteresis loops in most cases. The only exception was MF(0.30), whose isotherm possessed a much wider hysteresis loop and a higher uptake at p/p^0 near saturation than without heat treatment. The heat treatment led to increased specific surface area for all pastes (Table 3). Since the open porosities ε increased due to the temperature treatment as well, the change of the hydraulic radius r_h was small in all cases except for PC2 + SF(0.25). As in the case of the non-heat treated pastes, no mensurable microporosity was found for any of the heat treated specimens.

It should be noted that there was no visible appearance of cracks in the surfaces of the membranes due to the heat treatment. Again,

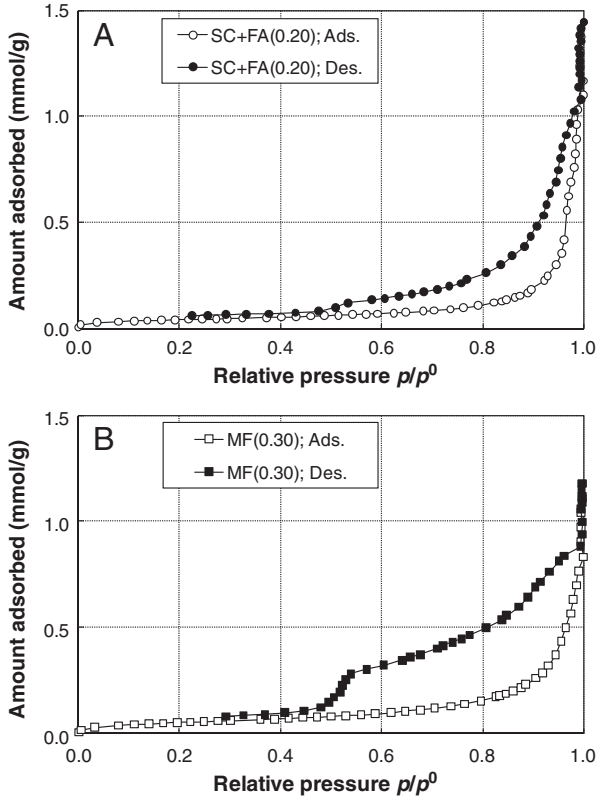

Fig. 3. Nitrogen adsorption isotherms of (A) non-heat treated paste SC + FA(0.20), and (B) non-heat treated paste MF(0.30).

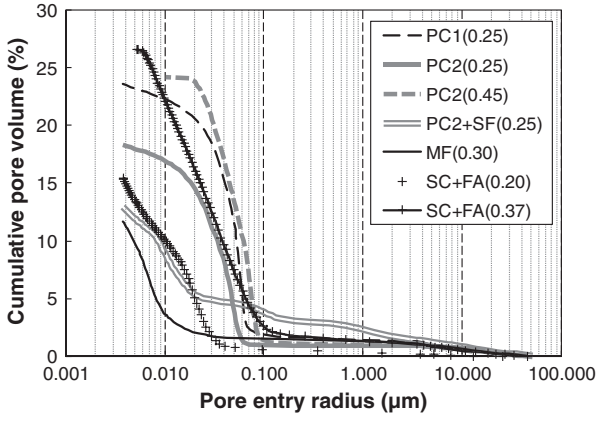

Fig. 4. Mercury porosimetry results of the heat treated cement pastes.

this is in accord with the observations of Farage et al. [11], who found that there was no formation of cracks in hcp slices of thickness 4 mm heated up to 300 °C, while cracks appeared in thicker slices.

4.3. Separation factors

The separation factors α_{H_2,CO_2} of the membranes ranged from 1.42 to 3.43 and exhibited a strong dependence on the mix-design of the pastes and on temperature. It can be seen from Fig. 5 that a low w/b and the use of pozzolanic materials led to higher separation factors of the membranes. Comparison with the results discussed in Sections 4.1 and 4.2 shows that in general a finer pore structure and a high separation factor occurred with the same membranes.

Fig. 6 shows a plot of the hydraulic radii and the separation factors of the tested membranes. The hydraulic radius is a common measure of the average width of a pore system, independent of the shape of its pores. However, no interrelation between r_h and α_{H_2,CO_2} could be observed. Instead, the separation factors tended to depend on the threshold radii of the pastes: in general a smaller r_{thr} led to a higher α_{H_2,CO_2} for all temperatures (Fig. 7). This is equally true for the membrane MF(0.30), which exhibited a high fraction of its pore volume behind pore entrances of $r_P \leq 2.5$ nm, much smaller than its threshold radius.

According to Diamond [32] the threshold radius of hcp represents the width of "choke points" that allow breakthrough of mercury in most of its pore space during the mercury porosimetry experiment. That means that the threshold radius is a measure of the size of the controlling constrictions in the pore channels that percolate throughout the paste; it may be envisaged as the radius of the greatest sphere that is able to pass through the paste on at least one path. Based on the results outlined above, it appears that these choke points determine the separation factors of the hcp membranes, while the average pore width has no influence on the separation factors. Furthermore, the existence of a high fraction of pore volume behind entrances much smaller than the threshold radius – as is the case with MF(0.30) – does not alter this situation; apparently these pores do not contribute much to the diffusional mass transport.

Because the threshold radii changed only slightly due to the heat treatment, there was a correlation between the separation factors of the membranes and the threshold radii of the cement pastes before heat treatment as well, although the scattering of the data was more marked than in Fig. 7.

4.4. Knudsen numbers

Since the separation factors of the membranes depended on the width of the controlling constrictions of the pore system – i.e. the threshold radii of the cement pastes – it can be concluded that virtually all gas molecules have to pass through these constrictions when moving through the membrane, in a comparable manner as mercury does during the mercury porosimetry experiments. Therefore, the threshold radii after heat treatment were taken as the basis for calculating the Knudsen numbers of the pastes.

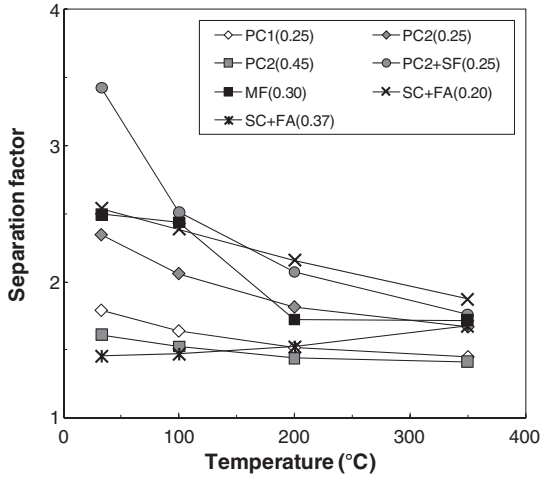

Fig. 5. Separation factors of the membranes.

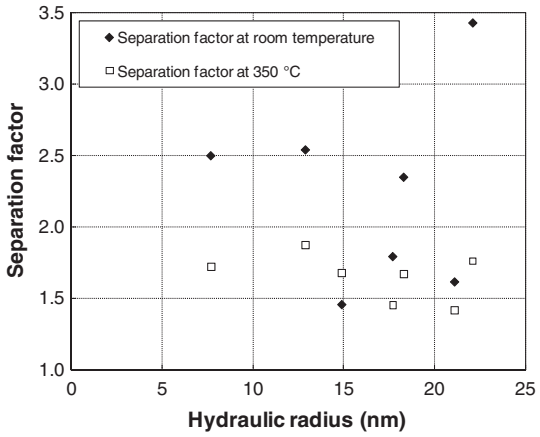

Fig. 6. Plot of hydraulic radii of heat treated cement pastes versus separation factors of the corresponding membranes. For clarity, the separation factors at 100 °C and 200 °C are not shown.

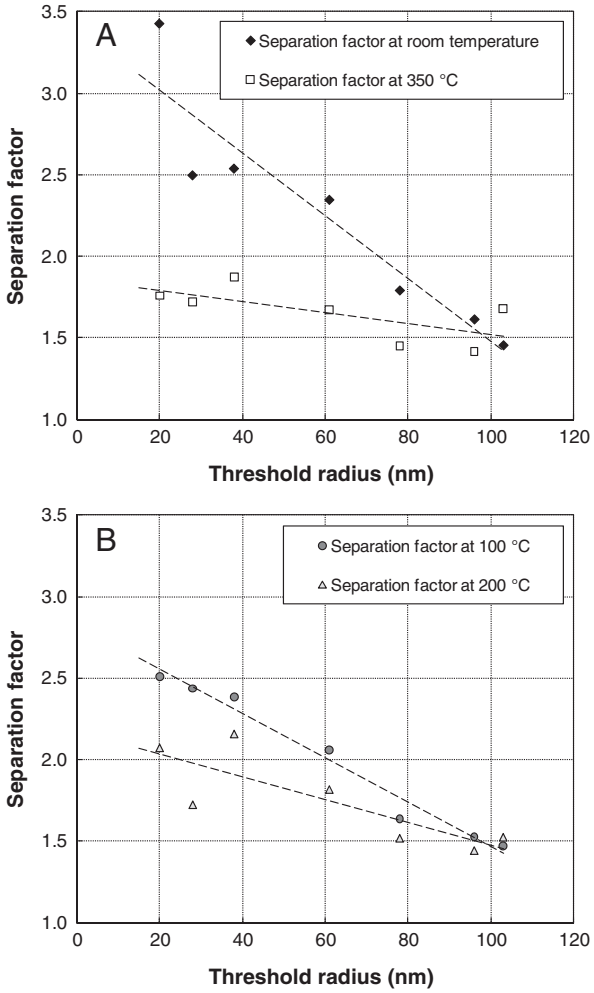

Fig. 7. Correlation between threshold radii of heat treated cement pastes and separation factors of the corresponding membranes (A) at room temperature and 350 °C, and (B) at 100 °C and 200 °C.

To calculate the average mean free path of the molecules in the gas mixture, the molecular diameter d_i in Eq. (1) was replaced by the average diameter d_{av}, estimated from

$$d_{av} = \sum_{i=1}^{3}\sum_{j=1}^{3}\left(\frac{d_i}{2}+\frac{d_j}{2}\right)x_i x_j, \tag{10}$$

where the indices $i, j = 1, 2, 3$ denote the gas species H_2, CO_2, N_2, respectively. Eq. (10) can be derived from considerations about the collision cross-sections of the different pairs of molecules and their relative occurrence in the mixture. The mole fractions of the gas species were taken as mean fractions in the system, i.e. $x_{H_2} = 0.249$, $x_{CO_2} = 0.251$, $x_{N_2} = 0.500$. The molecular diameters were calculated from the van der Waals constants b of the three gases [22] to be $d_{H_2} = 0.276$ nm, $d_{CO_2} = 0.323$ nm, $d_{N_2} = 0.314$ nm. These numbers may be compared with the Lennard–Jones collision diameters of the gases $\sigma_{H_2} = 0.2915$ nm, $\sigma_{CO_2} = 0.3996$ nm, $\sigma_{N_2} = 0.3667$ nm [23]. With the values given above, d_{av} was calculated to be 0.307 nm and the mean free path of the molecules was calculated to lie between 96.1 nm at 32 °C and 195.6 nm at 350 °C.

Fig. 8 shows a plot of the calculated Knudsen numbers. The Knudsen numbers ranged from 0.47 at room temperature to 4.89 at 350 °C with higher Knudsen numbers for the pastes with smaller threshold radius. That means that diffusion in the controlling constrictions of the pore systems took place in the transient regime between Knudsen diffusion and bulk diffusion, Knudsen diffusion predominating in the membranes with smaller r_{thr}, i.e. with a finer pore structure.

It should be noted that the Knudsen numbers might be even higher, since in the analysis of the mercury porosimetry results the contact angle between mercury and hcp was assumed to be 141.3°, whereas Winslow and Diamond [31] arrived at $\theta = 117°$. Thus, the threshold radii might be smaller than calculated here by about 42% and accordingly, the Knudsen numbers would rise.

4.5. Temperature dependence of diffusion coefficients

To further assess the diffusion mechanism, the temperature dependence of the effective diffusion coefficients of the membranes was analysed. From the recorded gas compositions at the permeate side outlet and the feed side outlet the effective diffusion coefficients D_i^{eff} were calculated according to Eq. (7). Since the compositions are changing continuously while the gases flow across the membrane, the average mole fractions of the three components were not known precisely. Therefore, the differences in the mole fractions had to be calculated with the simplifying assumption that the average mole fraction of each component on either side of the membrane was the arithmetic mean of the mole fractions at the corresponding inlet and outlet.

Typical examples of the dependence of D_i^{eff} on temperature are shown in Fig. 9; the other membranes possessed similar D_i^{eff} versus T plots. Fig. 9 shows that for H_2 and N_2 the curves can approximately be fitted by $D_i^{eff} = \text{const.} \cdot T^{0.5}$. The temperature dependence of the effective diffusion coefficient of CO_2 differed more widely between the membranes, being described by $D_{CO_2}^{eff} = \text{const.} \cdot T^{0.3\ldots1.3}$.

Since according to Eqs. (5), (6) and (7) the effective diffusion coefficients for Knudsen diffusion would be given by $D_i^{eff} = \text{const.} \cdot T^{0.5}$, the above results can be reconciled with the conclusions drawn in the previous section. In the case of bulk diffusion, however, the situation is more complex. In that regime, the fluxes, mole fractions and mole fraction gradients are all interrelated according to Eqs. (2) and (3). Furthermore, under the given experimental conditions, the mole fraction gradients depend on the fluxes of the gases. Thus, the temperature dependence of the fluxes – and consequently of the D_i^{eff} – is not amenable to a simple analysis. Consequently, no definite conclusions on the relative importance of bulk diffusion and Knudsen diffusion can be drawn from the measured temperature dependence of the effective diffusion coefficients alone. Possibly, the differing exponents of T in the effective diffusion coefficients of CO_2 are related to the influence of bulk diffusion. The contribution of surface diffusion to mass transport in the membranes is considered to be small, since the specific surface areas of all pastes were low.

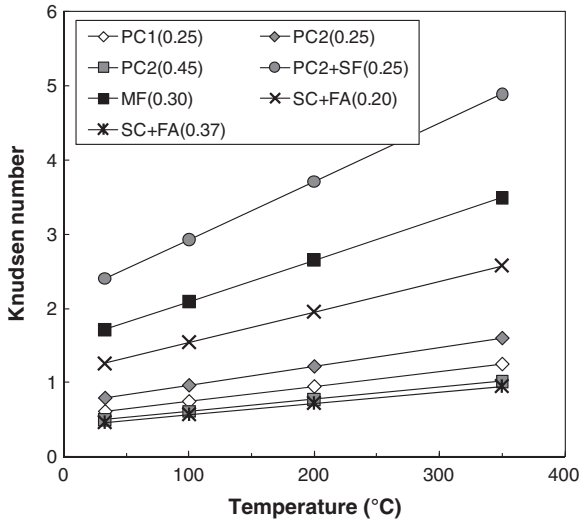

Fig. 8. Knudsen numbers of the membranes. Pore diameters in $Kn = \lambda/d_P$ were calculated from the threshold radii of the pastes.

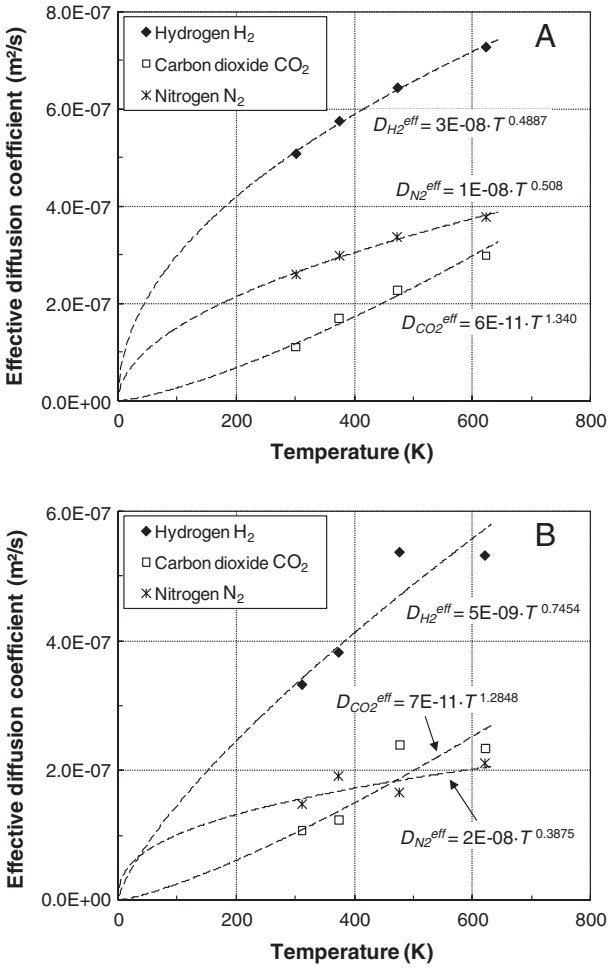

Fig. 9. Plot of effective diffusion coefficients versus temperature for (A) membrane PC2 + SF(0.25), and (B) membrane MF(0.30).

5. Discussion

Since the threshold radius reflects the intrinsic pore system of hcp (capillary and gel pores) [31,32], the choice of taking r_{thr} as basis for the calculation of the Knudsen numbers rests on the assumption that the character of gaseous diffusion in the membranes was determined by this pore system, i.e. it was assumed that this intrinsic pore system could be completely bypassed by the gas molecules only on few paths, if at all. In addition to capillary and gel pores, concretes, mortars and cement pastes generally contain air voids with diameters of approximately 10–500 μm [32] as well as microcracks, induced by self-desiccation and drying shrinkage [30,47–49]. These voids and cracks increase the diffusivity of cement-based materials by lowering their effective thickness; in addition, air voids cause some heterogeneities at the air void-paste interface, comparable to the ITZ adjacent to aggregates in concrete [50]. However, air voids exist as isolated pores in the hcp matrix [32,50], while being one to two orders of magnitude smaller than the thickness of the membranes employed in the current study. Furthermore, according to Hwang and Young [47], drying of 1–2 mm thick unrestrained hcp slices induces shrinkage cracking only at their surfaces, i.e. the shrinkage cracks do not traverse or percolate the slices. Analogous results were reported by Bisschop and van Mier [49] for much larger specimens. Consistent with these observations, Wong et al. [30] found that dried cement pastes possess much lower transport coefficients than what would be expected from the transport coefficients of corresponding mortars and concretes (in which the microcracks might well be interconnected throughout the entire specimen; cf. Ref. [49]). Heat treatment may also cause microcracking of cementitious materials. However, in contrast to what is observed with mortars [12], Farage et al. [11] found that heating hcp to 300 °C causes no significant increase of the gas permeability as compared to permeability after 80 °C treatment; in addition, the elastic modulus of hcp was not much decreased in this temperature range, which is another sign of only limited cracking. Furthermore, this limited damage seemed to be restricted to the drying surfaces of the specimens and, as was mentioned above, to be even less significant for thin specimens. From these considerations it is apparent that neither air voids nor microcracks formed traversing paths in the membranes — the latter due to the absence of aggregates. Thus, there is additional support for the assumption made in the calculation of the Knudsen numbers, previously justified only with the dependence of α_{H_2,CO_2} on r_{thr}. Since the hydration of hcp – in particular that of pastes containing slag and/or fly ash – proceeds significantly after 28 days, thereby leading to a finer intrinsic pore structure of the paste, it follows that prolonged curing of the membranes would have led to somewhat smaller threshold radii and, in turn, to higher separation factors. The extent to which these changes are expected to occur depends on the binder type and w/b of the membrane.

Regarding the transport properties of cementitious materials in general, the present study represents a confirmation and extension of previous experimental work on the gas transport mechanisms in concrete, mortar and cement paste [7,9–12]. We presented additional evidence of Knudsen diffusion in the pores of hcp and showed that, in fact, the coefficient of gaseous diffusion in these materials approximately obeys the temperature dependence, implied by the former. This has some implications for the mathematical treatment of transport processes in cementitious materials. The appropriate pressure and temperature dependence of the diffusion coefficients has to be used when results of laboratory measurements are to be extrapolated to specific service conditions, e.g. hot temperatures. Also, as has already been recognised [8], the interplay of Knudsen and bulk diffusion should be the starting point for models of transport in cementitious materials and concrete durability (where carbon dioxide and oxygen diffusion are important). Furthermore, the degree to which Knudsen effects occur in gas diffusion experiments may serve to analyse microstructural damage in cementitious materials, similar to the approach of Lion et al. [12] using gas permeability measurements.

From the important role of Knudsen diffusion in finely porous hcp it follows that in general a separation of gases of low molecular weight from higher weight gases occurs in the pore system of hcp. This means that the separation of H_2 from a mixture of H_2, CO_2 and N_2 is possible, if a sweep gas other than N_2 is used. Thus, cement paste membranes with adjusted pore structure (small threshold radius) may be used to process the wood gasification product at temperatures higher than can be withstood by polymer membranes. However, the economic viability of these membranes in industrial applications depends on the gas fluxes and the surface area/volume ratio of the membrane modules [15,16], which are limited by the minimum membrane thickness achievable. The latter again is governed by the mechanical and thermal stability of the material and the occurrence of microcracks that traverse the membrane. Thus, future studies should investigate these parameters and develop feasible modules for the cement membranes.

6. Conclusions

In the present study it was shown that membranes made of cement paste yield separation factors up to 3.43 for a H_2/CO_2 mixture. However, this maximum separation factor occurred at room temperature, when polymer membranes can be used as well. In general, the separation factor decreased with increasing temperature; the highest result at 350 °C was $\alpha_{H_2,CO_2} = 1.87$.

The separation factors of the cement paste membranes exhibited an approximately linear dependence on the threshold radii of the pastes for all temperatures, smaller threshold radii leading to higher separation factors. This implies that the size of the constrictions of the percolating pore channels control the separation factors. The Knudsen numbers of these constrictions show that gas transport in these channels takes place in the transient regime between Knudsen diffusion and bulk diffusion, in the case of the smallest threshold radii, Knudsen diffusion prevails. These conclusions are in line with the temperature dependence of the measured effective diffusion coefficients, which in general can be described approximately by $T^{0.5}$.

The prevalence of Knudsen diffusion in finely porous hcp means that, in principle, this material can be used in gas separation applications. However, before cement paste membranes can be used for industrial operations, further efforts are required. The results of the current study furthermore emphasise the importance of taking into account Knudsen effects, such as the modified temperature dependence of diffusion coefficients, when modelling gaseous diffusion in cementitious materials.

Acknowledgements

This work was funded by the Agency for Renewable Resources (FNR) under grant no. 22010502. One of the authors (G.J.G.G.) would like to thank Dr Roland Herr for the valuable discussions.

References

[1] J.J. Beaudoin, R.F. Feldman, P.J. Tumidajski, Pore structure of hardened Portland cement pastes and its influence on properties, Adv. Cem. Based Mater. 1 (1994) 224–236.
[2] H.F.W. Taylor, Cement Chemistry, 2nd ed. Thomas Telford, London, 1997.
[3] R. Krishna, J.A. Wesselingh, The Maxwell–Stefan approach to mass transfer, Chem. Eng. Sci. 52 (1997) 861–911.
[4] H.E. Schwiete, H.J. Bohme, U. Ludwig, Measuring gas diffusion for the valuation of open porosity on mortars and concrete, Mater. Struct. 2 (1969) 43–48.
[5] H.E. Schwiete, H.J. Böhme, Bestimmung der effektiven Porosität von Beton durch Gasdiffusionsmessungen, Zem. Kalk Gips 23 (1970) 125–134.
[6] G.M. Därr, U. Ludwig, Determination of permeable porosity, Mater. Struct. 6 (1973) 185–190.
[7] J. Sercombe, R. Vidal, C. Gallé, F. Adenot, Experimental study of gas diffusion in cement paste, Cem. Concr. Res. 37 (2007) 579–588.
[8] T.H. Vu, F. Frizon, S. Lorente, Architecture for gas transport through cementitious materials, J. Phys. D: Appl. Phys. 42 (2009) 105501.
[9] A. Abbas, M. Carcasses, J.-P. Ollivier, Gas permeability of concrete in relation to its degree of saturation, Mater. Struct. 32 (1999) 3–8.

[10] H. Loosveldt, Z. Lafhaj, F. Skoczylas, Experimental study of gas and liquid permeability of a mortar, Cem. Concr. Res. 32 (2002) 1357–1363.
[11] M.C.R. Farage, J. Sercombe, C. Gallé, Rehydration and microstructure of cement paste after heating at temperatures up to 300 °C, Cem. Concr. Res. 33 (2003) 1047–1056.
[12] M. Lion, F. Skoczylas, Z. Lafhaj, M. Sersar, Experimental study on a mortar. Temperature effects on porosity and permeability. Residual properties or direct measurements under temperature, Cem. Concr. Res. 35 (2005) 1937–1942.
[13] A.V. Bridgwater, The technical and economic feasibility of biomass gasification for power generation, Fuel 74 (1995) 631–653.
[14] S. Gerber, F. Behrendt, M. Oevermann, An Eulerian modeling approach of wood gasification in a bubbling fluidized bed reactor using char as bed material, Fuel 89 (2010) 2903–2917.
[15] R.W. Baker, Membrane Technology and Applications, 2nd ed. Wiley, Chichester, 2004.
[16] T. Melin, R. Rautenbach, Membranverfahren: Grundlagen der Modul- und Anlagenauslegung, 3 rd ed. Springer, Berlin, 2007.
[17] P. Bernardo, E. Drioli, G. Golemme, Membrane gas separation: a review/state of art, Ind. Eng. Chem. Res. 48 (2009) 4638–4663.
[18] J. Caro, M. Noack, P. Kölsch, R. Schäfer, Zeolite membranes — state of their development and perspective, Microporous Mesoporous Mater. 38 (2000) 3–24.
[19] J. Caro, M. Noack, Zeolite membranes — recent developments and progress, Microporous Mesoporous Mater. 115 (2008) 215–233.
[20] R.W. Baker, Future directions of membrane gas separation technology, Ind. Eng. Chem. Res. 41 (2002) 1393–1411.
[21] K. Keizer, R.J.R. Uhlhorn, V.T. Zaspalis, A.J. Burggraaf, Transport and related (gas and vapour) separation in ceramic membranes, Key Eng. Mater. 61–62 (1991) 143–154.
[22] G. Wedler, Lehrbuch der Physikalischen Chemie, 5th ed. Wiley-VCH, Weinheim, 2004.
[23] R.B. Bird, W.E. Stewart, E.N. Lightfoot, Transport Phenomena, revised 2nd ed. Wiley, New York, 2007.
[24] P.J.A.M. Kerkhof, M.A.M. Geboers, Analysis and extension of the theory of multicomponent fluid diffusion, Chem. Eng. Sci. 60 (2005) 3129–3167.
[25] N. Epstein, On tortuosity and the tortuosity factor in flow and diffusion through porous media, Chem. Eng. Sci. 44 (1989) 777–779.
[26] G.R. Gavalas, Diffusion in microporous membranes: measurements and modeling, Ind. Eng. Chem. Res. 47 (2008) 5797–5811.
[27] H.-J. Wierig, Die Carbonatisierung des Betons, Naturstein Ind. 22 (1986) 26–35.
[28] H. Strathmann, C.M. Bell, W. Gudernatsch, K. Kimmerle, Die Entwicklung von lösungsmittelselektiven Membranen und ihre Anwendung in der Gastrennung und Pervaporation, Chem. Ing. Tech. 60 (1988) 590–603.
[29] J.J. Kollek, The determination of the permeability of concrete to oxygen by the Cembureau method — a recommendation, Mater. Struct. 22 (1989) 225–230.
[30] H.S. Wong, M. Zobel, N.R. Buenfeld, R.W. Zimmerman, Influence of the interfacial transition zone and microcracking on the diffusivity, permeability and sorptivity of cement-based materials after drying, Mag. Concr. Res. 61 (2009) 571–589.
[31] D.N. Winslow, S. Diamond, A mercury porosimetry study of the evolution of porosity in Portland cement, J. Mater. (ASTM) 5 (1970) 564–585.
[32] S. Diamond, Mercury porosimetry: an inappropriate method for the measurement of pore size distributions in cement-based materials, Cem. Concr. Res. 30 (2000) 1517–1525.
[33] R. Härdtl, Veränderungen des Betongefüges durch die Wirkung von Steinkohlenflugasche und ihr Einfluß auf die Betoneigenschaften, Schriftenr. Deutscher Ausschuss für Stahlbeton, 448, Beuth, Berlin, 1995.
[34] B.C. Lippens, J.H. de Boer, Studies on pore systems in catalysts: V. The t method, J. Catal. 4 (1965) 319–323.
[35] K.S.W. Sing, Assessment of microporosity, Chem. Ind. (London) (1967) 829–830.
[36] B.C. Lippens, B.G. Linsen, J.H. de Boer, Studies on pore systems in catalysts: I. The adsorption of nitrogen; apparatus and calculation, J. Catal. 3 (1964) 32–37.
[37] S. Brunauer, P.H. Emmet, E. Teller, Adsorption of gases in multimolecular layers, J. Am. Chem. Soc. 60 (1938) 309–319.
[38] F. Rouquerol, J. Rouquerol, K.S.W. Sing, Adsorption by Powders & Porous Solids: Principles, Methodology and Applications, Academic Press, San Diego, 1999.
[39] N.A. Seaton, Determination of the connectivity of porous solids from nitrogen sorption measurements, Chem. Eng. Sci. 46 (1991) 1895–1909.
[40] P.I. Ravikovitch, A.V. Neimark, Experimental confirmation of different mechanisms of evaporation from ink-bottle type pores: equilibrium, pore blocking, and cavitation, Langmuir 18 (2002) 9830–9837.
[41] A. Vishnyakov, A.V. Neimark, Monte Carlo simulation test of pore blocking effects, Langmuir 19 (2003) 3240–3247.
[42] E.E. Bodor, J. Skalny, S. Brunauer, J. Hagymassy, M. Yudenfreund, Pore structures of hydrated calcium silicates and Portland cements by nitrogen adsorption, J. Colloid Interface Sci. 34 (1970) 560–570.
[43] R.S. Mikhail, S.A. Abo-El-Enein, Studies on water and nitrogen adsorption on hardened cement pastes: I. Development of surface in low porosity pastes, Cem. Concr. Res. 2 (1972) 401–414.
[44] M.C. Garci Juenger, H.M. Jennings, The use of nitrogen to assess the microstructure of cement paste, Cem. Concr. Res. 31 (2001) 883–892.
[45] A. Korpa, R. Trettin, The influence of different drying methods on cement paste microstructures as reflected by gas adsorption: comparison between freeze-drying (F-drying), D-drying, P-drying and oven-drying methods, Cem. Concr. Res. 36 (2006) 634–649.
[46] J.J. Thomas, J. Hsieh, H.M. Jennings, Effect of carbonation on the nitrogen BET surface area of hardened Portland cement paste, Adv. Cem. Based Mater. 3 (1996) 76–80.
[47] C.-L. Hwang, J.F. Young, Drying shrinkage of Portland cement pastes: I. Microcracking during drying, Cem. Concr. Res. 14 (1984) 585–594.
[48] K.O. Kjellsen, H.M. Jennings, Observations of microcracking in cement paste upon drying and rewetting by environmental scanning electron microscopy, Adv. Cem. Based Mater. 3 (1996) 14–19.
[49] J. Bisschop, J.G.M. van Mier, Effect of aggregates on drying shrinkage microcracking in cement-based composites, Mater. Struct. 35 (2002) 453–461.
[50] H.S. Wong, A.M. Pappas, R.W. Zimmerman, N.R. Buenfeld, Effect of entrained air voids on the microstructure and mass transport properties of concrete, Cem. Concr. Res. 41 (2011) 1067–1077.